

# The Turbulence Structure in Bubbly Channel Flow

Akiko FUJIWARA\*, Soohyun SO\*\*, Shu TAKAGI\*\*, Koichi HISHIDA\* and Yoichiro MATSUMOTO\*\*

\*Department of System Design Engineering, Keio University,

3-14-1 Hiyoshi, Kohoku-ku, Yokohama, 223-8522, Japan

\*\*Department of Mechanical Engineering, The university of Tokyo,

7-3-1 Hongo, Bunkyo-ku, Tokyo, 113-8656, Japan

The objective of the present study is to investigate the mechanism of turbulence modification by bubbles in vertical channel upward flows. The experiment was conducted with various void fractions and Reynolds number. Liquid phase velocity is measured by the Particle Image Velocimetry with fluorescent tracer particles (PIV/LIF) and the Laser Doppler Velocimetry (LDV), respectively. By using image-processing technique, bubble size and distribution are observed. The bubbles are strongly accumulated near the wall and slide up along the wall in the channel. The high concentrated bubbles in the vicinity of the wall disturb the transport of turbulence energy, thus the fluctuation velocity is remarkably reduced at the wide region of the channel center. Moreover, in the middle of channel, the turbulence structure is governed by pseudo-turbulence induced by present bubbles.

## 1. Introduction

One of the most important aspects of dispersed two-phase flow is the interaction of the dispersed phase with turbulent flow. Knowledge of turbulent bubbly flow has direct impact on the performance of many engineering systems. Recently, it has also received attention on the study of the drag reduction of a ship. In gas-liquid bubbly flows past experiments indicated that turbulence augmentation and reduction depends on the void fraction and gas flow rate (Serizawa et al., 1975, Theofanous and Sullivan, 1982, Lance and Bataille, 1991) in pipe flow. However, substantial disagreements among these experimental results can be seen in spite of the experiments taken under apparently similar conditions. One of the reasons for this disagreement is considered that the mean and rms values of the bubble diameter are uncertain and different among these measurements. And the mechanism of turbulent modulation by bubbles is still unexplored. Due to a large number of the uncertain factors in the previous experiments, reliable information for the closure modeling of the bubbly turbulent flow is not obtained yet. At the first step of the closure modelings of the bubbly turbulent flow, it is necessary to perform the measurement under the simple and ideal conditions.

In the present study, the experiments of the bubbly turbulent flow in vertical channel were conducted to elucidate the mechanism of turbulence modification and the effect of bubble buoyancy. We have studied an upward bubbly flow with various void fraction and Reynolds number. In order to elucidate the turbulence modification mechanism without channel dependency, the flow structure in two kinds of channel were compared. One channel has square and the other has two-dimensional rectangular cross section. For the square channel liquid velocity is measured by Particle Image Velocimetry with fluorescent tracer particles (PIV/LIF). And for rectangular channel liquid velocity is measured by Laser Doppler Velocimetry (LDV), respectively. By using image-processing technique, bubble size and distribution are observed. In this paper, turbulence fluctuation and Reynolds stress profile is investigated.

## 2. Experiment method for square channel

### 2.1 Experimental apparatus and conditions

Figure 1 shows a schematic of experimental apparatus. Water as the test fluid was pumped up to the upper tank and flowed upward in the channel. At the bottom of the channel there is the air bubble generator also shown in Figure 1. It consists of 34 stainless pipes with an inside diameter 0.07mm and outside diameter 0.5mm. The air pressure and flow was controlled by a pressure gauge and flow meter. The test section is 1730mm high with a 50x50mm<sup>2</sup> cross-sectional area. The channel width  $2h$  is 50mm. The upward flow direction is taken to the  $x$ -axis and transverse direction is taken to the  $y$ -axis. The laser sheet for PIV to measure the liquid velocity entered at  $z/h=0$  and

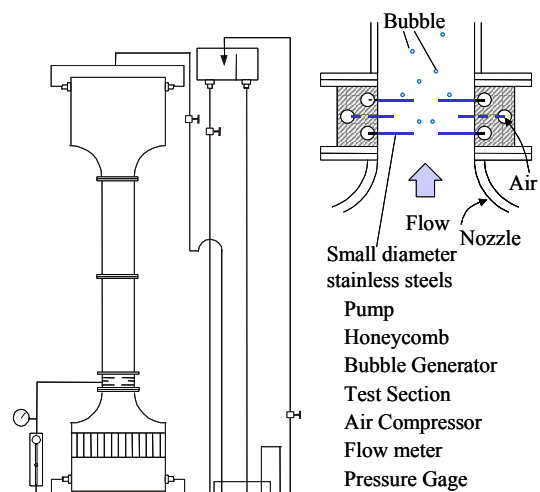


Fig. 1 Schematic of experimental apparatus (square channel).

illuminated an  $x$ - $y$  plane.

Table 1 shows the experimental conditions. All the experiments were run at a centerline single phase mean velocity of  $U_{s,c}=237\text{mm/sec}$ , corresponding to a Reynolds number of 10500 based on the channel width and bulk velocity. In order to compare the effect of the bubble diameter at same void fraction, nearly 60ppm of 3-Pentanol ( $\text{C}_5\text{H}_{11}\text{OH}$ ) are added as the surfactant.

Table 1. Experimental conditions (square channel).

Channel half width	$h$ [mm]	25
Bulk velocity (single phase)	$U_{s,b}$ [mm/s]	188
Channel Reynolds number	$Re_{2h}$	10500
Void fraction	$\alpha$ [%]	1.0
Estimated friction velocity	$u_\tau$ [mm/s]	11.7
Friction-velocity Reynolds number	$Re_\tau$	293

Figure 2 shows streamwise mean and fluctuation velocity profile of single phase with and no surfactant. The flow in the test section was fully developed turbulent flow, and there is no influence of the surfactant on the turbulence structure of single phase. Where  $U_{s,c}$  is the mean velocity at the center of the channel.

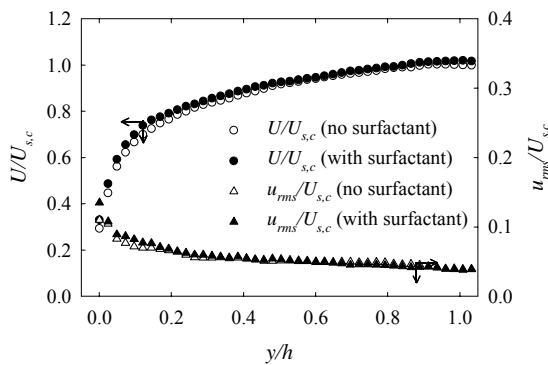


Fig. 2 Streamwise mean and fluctuation velocity profile (single phase in square channel).

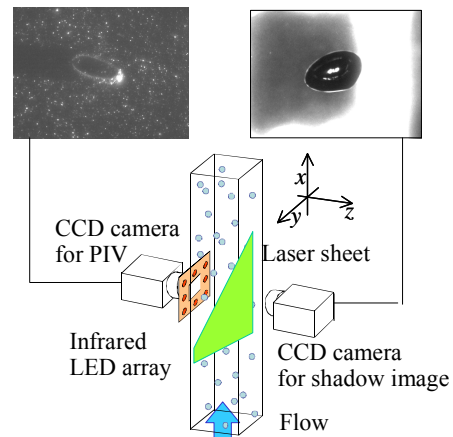


Fig. 3 Schematic of measurement system.

## 2.2 Measurement system

In order to measure the flow structure around the bubble, specifically to detect the interaction between the bubble motion and the flow field in time series, we implemented a PIV system previously described by Tokuhira et al. (1998) with the YAG laser ( $\lambda=532\text{nm}$ ). In order to avoid the high intensity light reflected from the bubbles surface which saturated the CCD devices, original fluorescent particles with Rhodamine-B as the fluorescent dye are applied as the tracer particles for PIV. The diameter of the tracer particles is approximately  $1\sim 10\ \mu\text{m}$  with a specific density of  $1.02\text{g/cm}^3$ . By attached a color filter, which cuts the reflection, the tracer images in the vicinity of the bubbles are obtained.

In order to capture the bubble's shape and position simultaneously, the projection technique using infrared LEDs ( $\lambda=800\sim 900\text{nm}$ ) as the light source was applied. The emitted light passes through a filter attached to the CCD camera and records both the shadow image of the bubble and the infrared-light.

Figure 3 depicts the arrangement consisting of two CCD cameras; one for PIV/LIF (left camera) and the other (right) for detecting bubble shape. A square "window" array of infrared LEDs permitted a view for PIV/LIF. In order to capture both the bubble shape and flow field simultaneously, the light sources and the two CCD cameras are synchronized.

## 3. Experiment method for rectangular channel

### 3.1 Experimental apparatus and conditions

The experimental facility is shown in Figure 4. The experiments are carried out in a vertical upward water channel sized  $40\times 400\times 2000\text{mm}^3$ , thus the aspect ratio is 10. And the experiment is conducted under two-dimensional flow. The bubble generator consisted of 474 stainless pipes

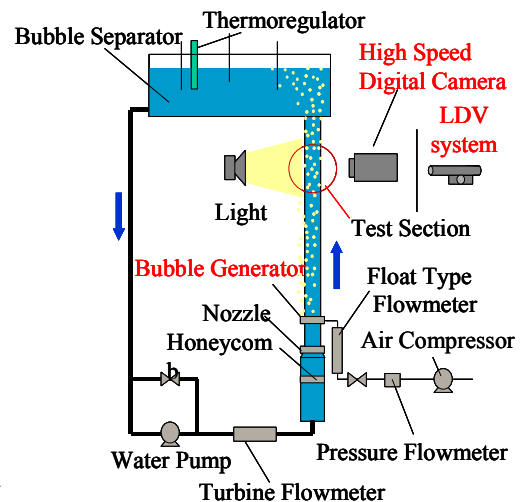


Fig. 4 Schematic of experimental apparatus (rectangular channel).

is installed above the inlet nozzle of the channel. The coordinate  $x$  denotes the streamwise direction in the test section and  $y$  denotes the transverse direction from the wall. The test section is 1600mm above the bubble generator.

The experimental conditions are shown in Table 2.

Table 2. Experimental conditions (rectangular channel).

Channel half width	$h$ [mm]	20			
Bulk velocity (single phase)	$U_{s,b}$ [mm/s]	29.0		92.0	
Channel Reynolds number	$Re_{2h}$	1350		4100	
Void fraction	$\alpha$ [%]	0.6	1.2	0.3	0.6
Estimated friction velocity	$u_\tau$ [mm/s]	---		5.9	
Friction-velocity Reynolds number	$Re_\tau$	---		147	

The Reynolds numbers based on the characteristic length of the channel width  $2h$  and the bulk velocity of the liquid phase are varied 1350 as laminar flow and 4100 as turbulent flow. At each condition in Table 2, 20ppm of 3-Pentanol was added as the surfactant to create small bubbles nearly sphere and avoid the effect of coalescence. To investigate the effect of the small amount of the surfactant on the fully developed turbulent channel flow, the streamwise mean velocity and turbulent fluctuations are measured for the single-phase flow by means of LDV system explained in the following section 3.2. Figure 5(a) shows the mean velocity profiles at  $Re=4100$  for the water flow and the flow with 3-pentanol. The difference by the surfactant is not observed in the figure, thus the amount of the surfactant is too small to modulate the turbulence structure. Figure 5(a) also compared with the result of DNS (Direct Numerical Simulation) at the Reynolds number based on the wall friction velocity  $Re_\tau$  of 150 (Kuroda et al., 1990). Two results show an excellent agreement with the DNS result. The turbulent fluctuations normalized by the wall friction velocity are shown in Figure 5(b). It is found that all fluctuations in the  $x$  and  $y$  direction are also in good agreement on the whole region.

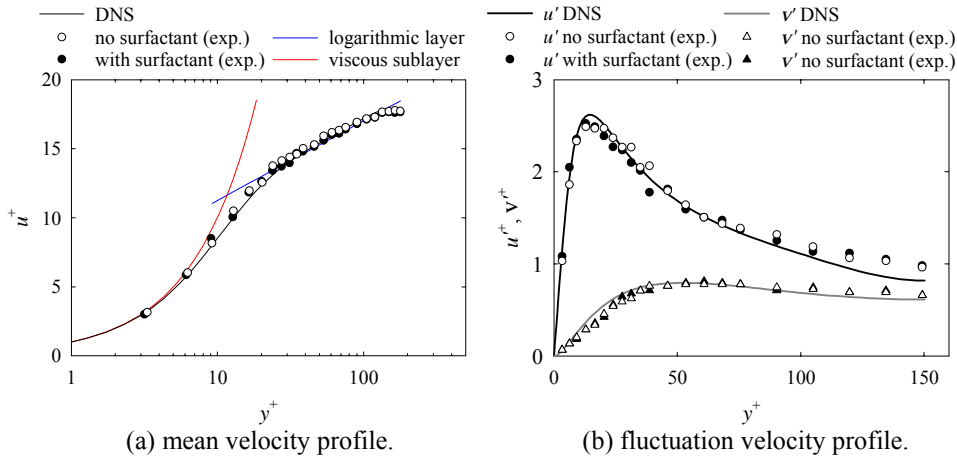


Fig. 5 Streamwise mean and fluctuation velocity profile compared with DNS data (single phase in rectangular channel).

### 3.2 Measurement system

2D LDV system (FLV 8835 type, KANOMAX) composed of air-cooling Argon-ion laser with a maximum output power of 300mW, is applied to measure the velocities of the liquid and dispersed phases. According to Theofanous and Sullivan (1982), the dense bubble region is formed near the wall. This creates the reduction of the inlet laser light and the scattering of the light. To avoid this reduction by the bubbles, the angle of inlet laser beam is given a slope of 3 degree. Spherical polystyrene particles of 8mm average diameter (density  $\rho=1.07\text{g/cm}^3$ ) are used as seeding particles for our LDV system.

In the two-phase flow, the liquid velocity is obtained from the information of seeding particles. However, discriminating the information of seeding particles from signal data of the two-phase in this kind of flow becomes important because dispersed bubbles also act as a scatter source for the laser systems. In the present study, the procedure of the discrimination is shown below:

- 1) Control the trigger level using the difference of a Doppler signal between seeding particles and bubbles.
- 2) Make the signal frequency of seeding particles overwhelms greatly compared with that of bubbles by the increase of the amount of seeding particles.
- 3) Remove velocity data of bubbles from velocity data distribution of the two-phase flow using the relative velocity between the liquid phase and bubbles.

Except for the extreme vicinity of the wall, the data noise due to the bubble motion can be discriminated from that of the two-phase flow by these methods. The sampling number is 3000 and the relative errors of the

mean and standard deviation are 1.8% and 2.5%, respectively (Yanta, 1973).

## 4. Results and discussions

### 4.1 Local void fraction and bubble diameter

Bubbles' diameter is evaluated from the shadow images projected by CCD camera. Figure 6 shows PDF of the bubble equivalent diameter  $D_{eq}$  in the square channel. The average  $D_{eq}$  is 0.99mm and standard deviation is 79% in the case of no surfactant. In contrary, average  $D_{eq}$  is 0.45mm and 15% of standard deviation in the case with surfactant. It indicates that by addition of surfactant, the bubbles leave from stainless pipes of the generator before growing large enough by shear force of flow and the bubbles have never be coalesced.

In order to characterize the presence of bubbles with respect to turbulence modification, the local void fraction was estimated under each condition in the square channel. Figure 7 shows the local void fraction  $\alpha'$  profile, where  $\alpha'$  is defined as the ratio of bubble area  $S_b$  to measurement area  $S$  defined by

$$\alpha' = \left\langle \sum_t S_b / S \right\rangle. \quad (4.1)$$

Where  $t$  is measurement time and  $\langle \rangle$  means time average. With considering the PDF of bubble diameter, Figure 7 indicated that many bubbles ascend near the wall ( $y/h \approx 0.1$ ) in the case of no surfactant. In contrary, small bubbles ( $D_{eq} \approx 0.5$ mm) dispersed uniformly in the flow with surfactant. By considering the stress balance in transverse direction, the governing factor to induce the lateral motion of the bubbles can be estimated. Roughly stress balance in transverse direction is written as

$$\frac{\partial \alpha_i \langle p_i \rangle}{\partial x} = - \frac{\partial}{\partial y} (\alpha_i \rho_l \langle v_i' v_i' \rangle). \quad (4.2)$$

Where,  $\alpha_i$ ,  $p_i$  and  $v_i'$  are volume fraction, pressure and fluctuation transverse velocity of the liquid phase. This equation shows the balance of the force induced by the transverse turbulence fluctuation velocity. Moreover, the velocity gradient  $\partial u / \partial y$  induced the lift force on the bubble such as Auton's lift force (Auton, 1987) written as

$$\mathbf{F}_L = C_L \frac{\pi}{6} D_{eq}^3 \rho_l (\mathbf{u}_g - \mathbf{u}_l) \times (\nabla \times \mathbf{u}_l). \quad (4.3)$$

$$C_L = 0.5$$

Where  $\rho_l$  and  $C_L$  are liquid phase density and lift force coefficient. It suggested the bubble slip velocity  $\mathbf{u}_g - \mathbf{u}_l$  have influence on the lift force efficiently. In the flow without surfactant, the slip velocity of large bubbles became faster than that of small bubbles in the flow with surfactant because of its buoyancy (Figure 8). By roughly estimation, the lift force induces the lateral motion of the bubbles dominantly in the case of no surfactant. And in case with surfactant, the slip velocity is too small to appear the effect of lift force distinctly, thus the different void fraction profile appeared in Figure 7.

For the rectangular channel, Figure 9 shows the PDF of the bubble diameter. In all cases 20ppm of 3-pentanoll is added as the surfactant. The average diameter is 1.1mm and the standard deviation is 15%. Bubbles are concentrated in the vicinity of the wall. We also observed that accumulated bubbles near the wall form clusters of 30-40mm length transversely and these clusters rise and

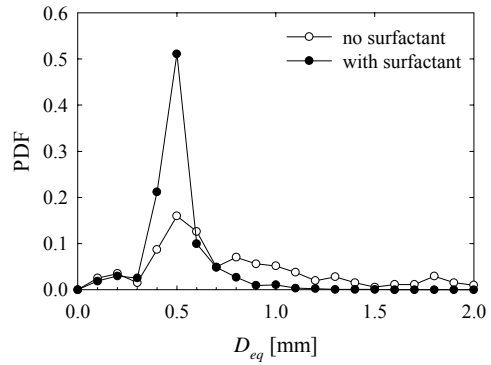


Fig. 6 PDF of the bubble equivalent diameter (square channel).

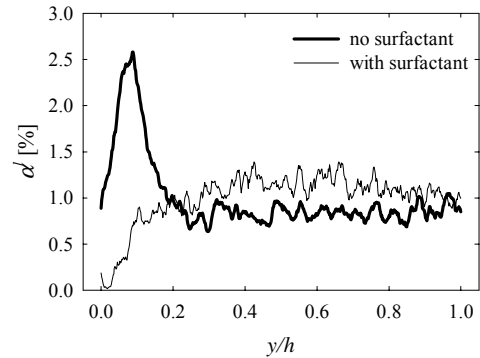


Fig. 7 The profile of local void fraction  $\alpha'$ .

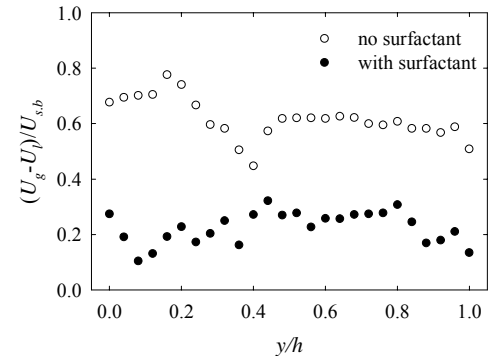


Fig. 8 Mean slip velocity of bubbles (rectangular channel).

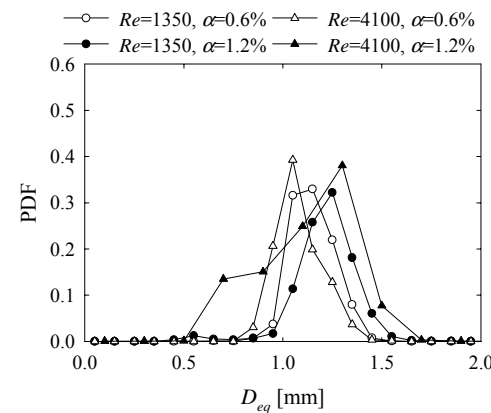


Fig. 9 PDF of the bubble equivalent diameter (rectangular channel).

oscillate like moving waves in the condition of  $Re=4100$ .

#### 4.2 Turbulence statistics of two-phase bubbly flow

Figure 10 shows profiles of mean streamwise velocity  $U$  and the fluctuation velocity  $u_{rms}$  of the liquid phase normalized by the bulk velocity of single phase  $U_{s,b}$  under each condition in the square channel. At the case of bubble uniform dispersion with surfactant,  $U$  profile is very similar to that in single phase. There is no apparent change in the mean flow in spite of the bubbles uniform dispersion with low bubble Reynolds number. On the other hand, at the case of high concentration of bubbles near the wall without surfactant,  $U$  is considerably accelerated along the wall and decelerated toward the middle channel region. It indicated that the bubbles ascending in the vicinity of the wall accelerated the flow. And mean streamwise velocity profile became flat.

In the case of bubble uniform dispersion, the streamwise fluctuation velocity increased in the whole region. The number density of bubble became large dramatically by the surfactant, and the wake interaction induced turbulence augmentation. On the other hand, in the case of high void fraction near the wall, fluctuation velocity is significantly enhanced near the wall. However, the turbulence reduction occurred remarkably in the region of  $y/h > 0.1$ . The point of  $y/h \approx 0.1$  is close to the peak of void fraction. These results suggested that the local void fraction has great influence on the turbulence modification in the same void fraction.

Figure 11 shows the profile of the Reynolds stress defined as  $-\langle u'v' \rangle$  in the rectangular channel. Where  $u'$  is streamwise fluctuation velocity. In the case of uniform dispersion of bubbles, Reynolds stress decrease near the wall of  $0.0 < y/h < 0.5$ , however the order is same as that of the single phase. In contrast, in the case of near wall concentration, Reynolds stress decreases dramatically in the whole area.

In the rectangular channel, the streamwise mean and fluctuation velocity profiles at  $Re=4100$  are shown in Figure 12. The mean velocity profiles of the liquid phase near the wall region are increased in the two phase flow. This is due to the acceleration effect of more densely concentrated bubbles near the wall. On the contrary, the profiles in the center of the channel are flattened as consequence of the acceleration effect of the liquid mean velocity by the bubble accumulations near the wall.

From the streamwise fluctuations in the vicinity of the wall, which corresponds to the more dense bubble region, are enhanced due to the pseudo-turbulence induced by the motion of the bubbles and the increase of liquid velocity gradient. Consequently, in Figure 12, the peak position of the fluctuation velocity exists closer to the wall in the two phase flow than that in the single phase flow and its position almost agrees with the dense bubble region. Also, in the region of  $0.1 < y/h < 0.6$ , lower values of turbulent fluctuations in the two phase flow are obtained lower values than those of the single phase flow. This reduction phenomenon has been observed by Serizawa et al. (1975), Wang et al. (1987) and Liu et al. (1993).

Figure 13 shows the Reynolds stress distribution of  $Re=4100$  in the rectangular channel. In the region of  $y/h > 0.2$ , Reynolds stress come close to zero due to the flattered mean velocity profiles.

The tendency of the fluctuation velocity and Reynolds

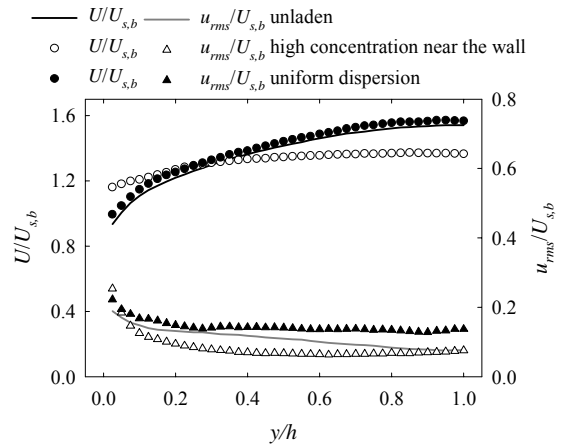


Fig. 10 Streamwise mean and fluctuation velocity profiles (square channel).

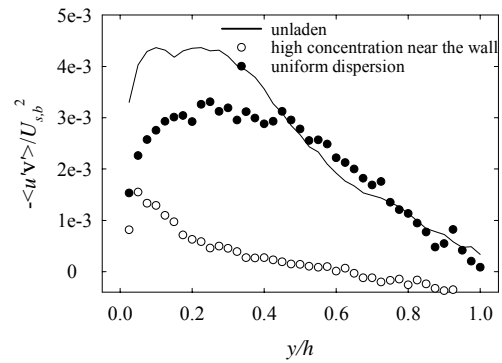


Fig. 11 Reynolds stress profiles (square channel).

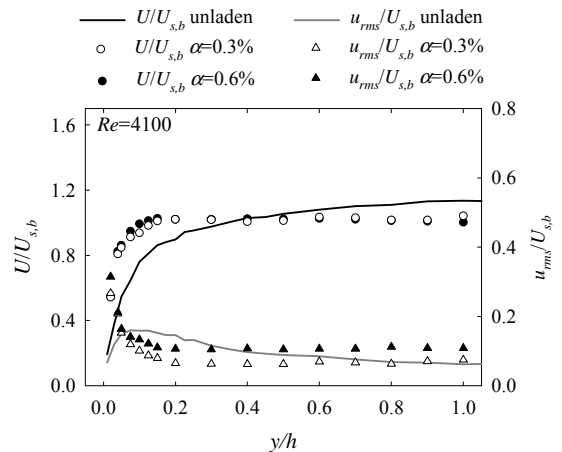


Fig. 12 Streamwise mean and fluctuation velocity profiles (rectangular channel).

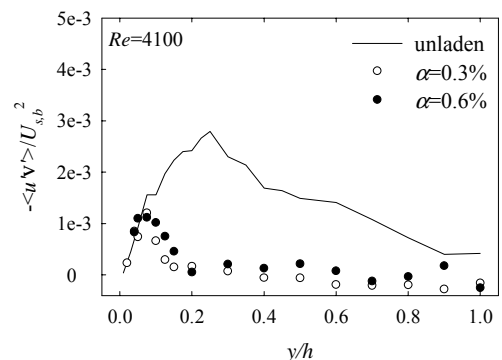


Fig. 13 Reynolds stress profiles (rectangular channel).

stress profile that reduced remarkably at the region from high void fraction to middle of the channel are appeared in both cases of square and rectangular channel. In order to define the effect of the pseudo-turbulence, figure 14 shows the mean and fluctuation velocity profile of  $Re=1350$  as laminar flow. By adding bubbles mean velocity is accelerated near the wall and the profile become flattered as shown same tendency in Figure 10 and 12. It indicated that the global mean velocity profile is not affected by unladen flow structure. Fluctuation velocity augmented drastically with the increase of void fraction. Figure 15 shows the fluctuation velocity profile of  $\alpha=0.6\%$  in both Reynolds number 1350 and 4100. At  $Re=4100$   $u_{rms}$  is larger than that at  $Re=1350$  as laminar flow. In contrary, in the middle of the channel ( $y/h>0.2$ )  $u_{rms}$  profile is in the same manner and no dependency of Reynolds number. It is indicated that the turbulence structure in the middle of the channel ( $y/h>0.2$ ) is induced by the ascending bubbles and there is no dependency of Reynolds number.

### 4.3 The mechanism of turbulence reduction

The most governing factor to reduce the streamwise turbulence intensity is the local void fraction. In the case of the high concentration of bubbles in the vicinity of the wall, the turbulence intensity reduce remarkably in the middle of the channel without dependency of the Reynolds number or the turbulence property.

In order to elucidate the macroscopic effect of the high concentrated bubbles, balance of stresses of the flow field is estimated. Roughly stress balance in stream wise direction is written as

$$\frac{\partial \alpha_i \langle p_i \rangle}{\partial x} + F_b = \frac{\partial}{\partial y} \left( \alpha_i \mu_i \frac{\partial \langle u_i \rangle}{\partial y} \right) - \frac{\partial}{\partial y} (\alpha_i \rho_i \langle u_i' v_i' \rangle), \quad (4.4)$$

and transverse direction has been already written as equation (4.2). Were,  $\mu_i$  and  $F_b$  are viscosity of the liquid phase and the term affected by the bubble buoyancy. By the roughly estimation, driving force induced by the pressure gradient has same order as the force induced by the buoyancy of the bubbles in streamwise direction. Generally the turbulence energy produced in the wall shear layer transported toward the middle of the channel by the momentum mixing. In the vertical channel flow as shown in Figure 16, the bubbles high concentrated in the vicinity of the wall drive the liquid phase in this region. And the turbulence energy transported from the wall is partly cancelled by this driving force in this region. Finally the turbulence energy cannot be transported toward the middle of the channel subsequently. Thus the fluctuation velocity and Reynolds stress reduce remarkably in the wide region of the channel center, and turbulence structure is induced by the present bubbles in the middle of the channel. It is indicated by the Figure 15 as pseudo turbulence for laminar-like flow conditions.

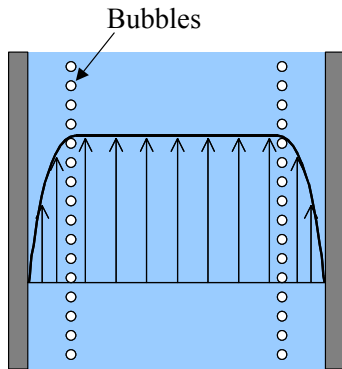


Fig. 17 The image of bubbly flow.

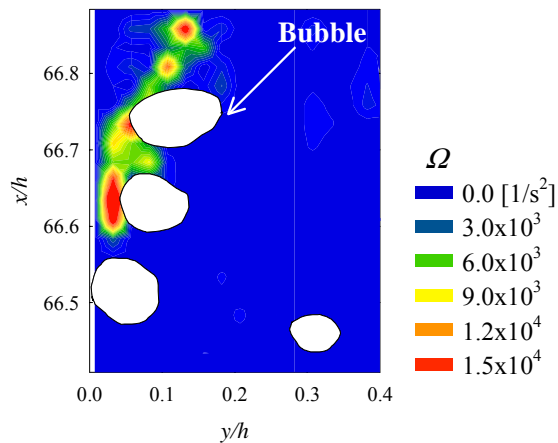


Fig. 17 Typical enstrophy contour near the wall (high void fraction near the wall in square channel).

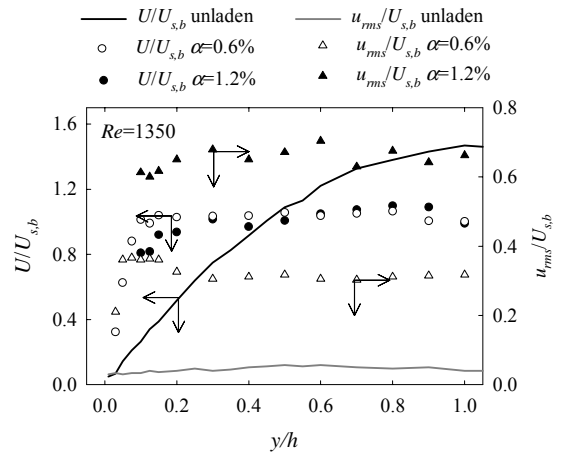


Fig. 14 Streamwise mean and fluctuation velocity profiles (rectangular channel).

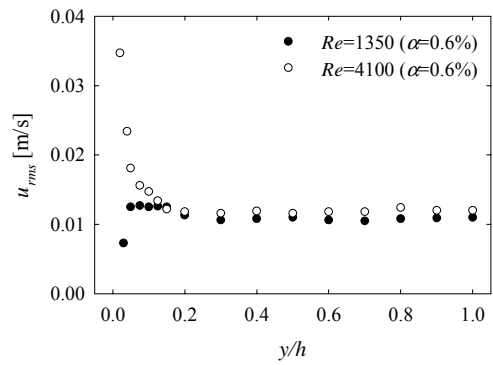


Fig. 15 Reynolds stress profile (rectangular channel).

The turbulence reduction mechanism affected by high concentrated bubbles can be confirmed from the local flow structure. Figure 17 shows instantaneous enstrophy contour around the bubbles in the square channel calculated for velocity vector fields measured by PIV. Enstrophy  $\Omega$  represents the stretching of vortex strings and indicates the turbulence fluctuation directly. Enstrophy is defined in terms of the intensity of vorticity fluctuation calculated written as

$$\Omega = (\omega_z - \langle \omega_z \rangle)^2. \quad (4.5)$$

Where  $\omega_z$  is local and instantaneous vorticity. In Figure 17 bubbles accumulated in the region of  $y/h \approx 0.1$ . The high intensity of  $\Omega$  is appeared in the region between the wall and bubbles. The interaction between the shear flow near the wall and the shear layer around the bubbles induced vorticity, thus high intensity of enstrophy appeared. Although in the region between bubbles and the middle of the channel there are no appearance of enstrophy.

## 5. Conclusions

The investigation of the fully developed vertical channel flow injected with dispersed bubbles has been performed using the PIV/LIF, LDV and image processing technique.

In the case of high void fraction distribution in the vicinity of the wall, turbulence intensity and Reynolds stress reduced dramatically at the wide region of the channel center without dependency of Reynolds number. High concentrated bubbles disturb the transport of turbulence energy produced in the wall shear layer and pseudo-turbulence induced by bubbles. Moreover, in the middle of channel, the turbulence structure is governed by pseudo-turbulence induced by present bubbles.

## Reference

- Auton, T.R. 1987, "The lift force in a spherical body in a rotational flow", *Journal of Fluid Mechanics*, **183**, pp.199-218.
- Kuroda, A., Kasagi, N. and Hirata, M. 1990, "A direct Numerical Simulation of the Turbulent Flow Between Two Parallel Walls: Turbulence Characteristics Near the Wall Without Mean Shear" 5th Symposium on Numerical Simulation of Turbulence, IIS of the University of Tokyo, pp. 1-5.
- Lance, M. and Bataille, J. 1991, "Turbulence in the liquid phase of a uniform bubbly air-water flow", *J. Fluid Mech.*, **222**, pp. 95-118.
- Liu, T. J. and Bankoff, S. G. 1993, "Structure of air-water bubbly flow in an vertical pipe-I. Liquid mean velocity and turbulence measurements", *Int. J. Heat Mass Transfer*, **36-4**, pp. 1049-1060.
- Serizawa, A., Kataoka, I. and Michiyoshi, I. 1975, "Turbulence Structure of Air-Water Bubbly Flow- II. Local Properties", *Int. J. Multiphase Flow*, **2**, pp. 235-246.
- Theofanous, T. G., and Sullivan, J. 1982, "Turbulence in two-phase dispersed flows", *J. Fluid Mech.*, **116**, pp. 343-362.
- Tokuhiro, A., Maekawa, M., Iizuka, K., Hishida, K. and Maeda, M. 1998, "Turbulent flow past a bubble and an ellipsoid using shadow-image and PIV techniques", *International Journal of Multiphase Flow*, **24**, pp.1383-1406.
- Wang, S. K., Lee, S. J., Jones Jr, O. C. and Lathey Jr, R. T. 1987, "3-D Turbulence Structure and Phase Distribution Measurements in Bubbly Two-Phase Flows", *Int. J. Multiphase Flow*, **13-3**, pp. 327-343.
- Yanta, W. J. 1973, "Turbulence Measurements with a Laser Doppler Velocimeter", *Naval Ordnance Laboratory Report*, NOLTR-73-94.